Berezinskii-Kosterlitz-Thouless transitions in a ferromagnetic superfluid: Effects of axial magnetization

Andrew P. C. Underwood,[1] Andrew J. Groszek,[2,3] Xiaoquan Yu,[4,1] P. B. Blakie,[1] and L. A. Williamson[2]

[1]*Department of Physics, Centre for Quantum Science, and Dodd-Walls Centre for Photonic and Quantum Technologies, University of Otago, Dunedin 9016, New Zealand*

[2]*ARC Centre of Excellence for Engineered Quantum Systems, School of Mathematics and Physics, University of Queensland, Saint Lucia, Queensland 4072, Australia*

[3]*ARC Centre of Excellence in Future Low-Energy Electronics Technologies, School of Mathematics and Physics, University of Queensland, Saint Lucia, Queensland 4072, Australia*

[4]*Graduate School of China Academy of Engineering Physics, Beijing 100193, China*

(Received 3 April 2024; accepted 24 June 2024; published 12 July 2024)

An easy-plane ferromagnetic spin-1 Bose gas undergoes two Berezinskii-Kosterlitz-Thouless transitions, associated with mass and spin superfluidity, respectively. We study the effect of axial magnetization on the superfluid properties of this system. We find that nonzero axial magnetization couples mass and spin superflow, via a mechanism analogous to the Andreev-Bashkin effect present in two-component superfluids. With sufficiently large axial magnetization mass and spin superfluidity arise simultaneously. The crossover to this phase provides a finite-temperature generalization of the zero-temperature broken-axisymmetric to easy-axis transition. We present analytic relations connecting mass and spin superfluidity with experimentally observable coherence of the three spinor components and local magnetization.

DOI: 10.1103/PhysRevA.110.013311

I. INTRODUCTION

Spinor Bose gases possess a variety of ground-state phases that, in addition to global phase coherence, may exhibit nematic or ferromagnetic order [1–4]. Consequently, such gases provide a rich platform to study equilibrium and nonequilibrium properties of both quantum and thermal phase transitions [5–18]. In a two-dimensional (2D) gas, thermal fluctuations preclude the formation of long-range order [19,20]; however, systems may still exhibit Berezinskii-Kosterlitz-Thouless (BKT) type transitions [21–23]. In spinor Bose gases, the interplay between spin and gauge symmetry can give rise to different BKT transitions and associated superfluid phases [24–29].

A spin-1 Bose gas in the easy-plane ferromagnetic phase exhibits distinct superflow of both mass and spin currents, corresponding to U(1) gauge and SO(2) spin-rotational symmetries, respectively [30,31]. The BKT transitions of this system have been studied previously; as temperature is decreased one observes first the emergence of mass superfluidity, followed at lower temperature by the emergence of spin superfluidity [28,29]. As the (conserved) axial magnetization is increased the local magnetization tilts out of the plane; see Fig. 1. Ultimately, the gas becomes axially magnetized, losing spin-rotational symmetry. Here, in the easy-axis-ferromagnetic phase, superfluidity is akin to that of a single-component superfluid, with any superflow corresponding solely to the U(1) gauge symmetry. The nature of the superfluidity as the system transitions from an easy-plane through to an easy-axis-ferromagnetic system has not been explored.

In this paper we investigate the effect of increasing axial magnetization on the superfluid properties of a ferromagnetic 2D spin-1 Bose gas. We utilize a stochastic Gross-Pitaevskii model [33–37], controlling the axial magnetization via the inclusion of a nonzero magnetic potential. With nonzero axial magnetization, mass and spin superfluidity are no longer independent quantities due to spin-gauge coupling [1,38]. This motivates the introduction of a third superfluid quantity simultaneously describing superflow of mass and spin currents, analogous to the superfluid drag present in two-component superfluids [39–42]. We find that the spin superfluid transition temperature increases with increasing axial magnetization, eventually coinciding with the mass superfluid transition temperature. This equality of mass and spin superfluid transition temperatures occurs while the gas possesses only partial axial magnetization. We connect superfluidity with coherence in the individual spin components and in the transverse spin, finding analytic relations between superfluid densities and the algebraic decay of correlations. Our results give insight into the rich superfluid behavior possible in spinor systems and pave the way for experimental observation.

II. FORMALISM

A. System

We consider a 2D spin-1 Bose gas with low-energy macroscopically occupied modes described by a three-component classical field $\Psi = [\psi_1, \psi_0, \psi_{-1}]^{\mathrm{T}}$. The components ψ_m denote the amplitudes of the $m \in \{1, 0, -1\}$ magnetic sublevels.

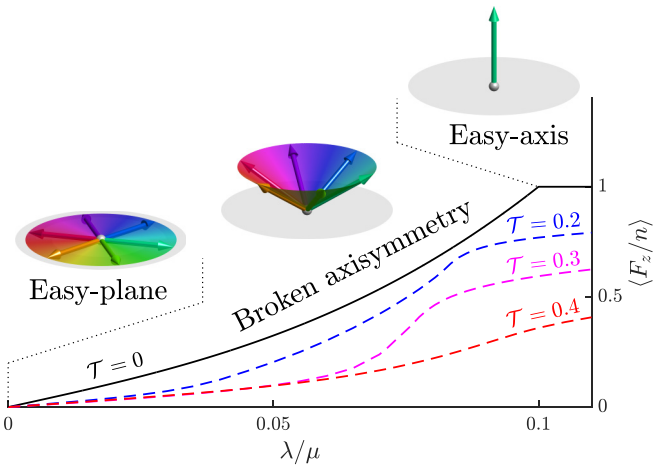

FIG. 1. Axial magnetization as a function of temperature $\mathcal{T}$ and magnetic potential λ in a ferromagnetic spin-1 Bose gas, along with schematics of corresponding zero-temperature phases. The transition from the broken axisymmetric to easy-axis phase occurs via a second-order phase transition at zero temperature [32]; see Eq. (2). This is modified at finite temperature [dashed lines, computed from Eq. (12)], where an understanding of the phases requires study of the system superfluid properties.

The system energy is [1,2]

$$E = \int d\mathbf{r}\left[\Psi^\dagger\left(-\frac{\hbar^2\nabla^2}{2M}\mathbb{1} + qf_z^2\right)\Psi + \frac{g_n}{2}n^2 + \frac{g_s}{2}|\mathbf{F}|^2\right], \tag{1}$$

where M denotes the atomic mass and q describes a uniform quadratic Zeeman shift arising from an external field along the z-spin axis [43]. The interactions are comprised of both density ($n = \Psi^\dagger\Psi$) and spin ($\mathbf{F} = \Psi^\dagger\mathbf{f}\Psi$) dependent terms, with respective 2D coupling constants $g_n > 0$ and g_s. Here $\mathbf{f} = (f_x, f_y, f_z)$ denotes the vector of spin-1 matrices. We consider ferromagnetic interactions $g_s < 0$, as realized in ultracold gases of ^{87}Rb [44,45] and ^{7}Li [46]. A linear Zeeman shift p has been omitted from Eq. (1), as this can be removed via the transformation $\Psi \to e^{-ipf_z t/\hbar}\Psi$.

The total energy is invariant under both the global phase shift $\Psi \to e^{i\theta}\Psi$ and z-spin rotation $\Psi \to e^{if_z\alpha}\Psi$. The corresponding conserved quantities are particle number $N = \int d\mathbf{r}\,\Psi^\dagger\Psi$ and z magnetization $M_z = \int d\mathbf{r}\,\Psi^\dagger f_z\Psi$, with associated chemical and magnetic potentials μ and λ, respectively. The zero-temperature phases of the system in the mean-field regime are the ground states of Eq. (1). Here we focus on the ferromagnetic phases, which are shown in Fig. 1 [32]. With $\lambda = 0$ and $0 < q < 2|g_s|n$ the axial magnetization is zero. Here, in addition to the breaking of U(1) gauge symmetry, the ground state breaks the SO(2) spin-rotational symmetry via the development of local magnetization transverse to the applied external field ("easy plane"). The effect of $0 < \lambda < q$ is the development of an axial component F_z of the local magnetization, which depends on λ and q as [32]

$$\frac{F_z}{n} = \frac{\lambda(\lambda^2 - q^2 + 2|g_s|nq)}{2|g_s|nq^2}. \tag{2}$$

The axial magnetization increases with λ until $\lambda = q$, at which point the system undergoes a second-order phase transition to the easy-axis ferromagnetic phase. For $\lambda \geqslant q$ the ground state is axially magnetized $F_z = n$. The discontinuity in $\partial\langle F_z\rangle/\partial\lambda$ at $\lambda = q$ is smoothed at finite temperature; see Fig. 1.

Although thermal fluctuations preclude symmetry breaking at nonzero temperature, quasi-long-range order below a BKT transition is still possible. In the easy-plane ferromagnetic gas ($\lambda = 0$) quasi-long-range order can be present in both global phase and transverse spin, arising via distinct BKT transitions. Consequently, this system exhibits superfluid flow of both mass and spin currents. In this paper we detail the superfluid properties of the ferromagnetic spin-1 Bose gas as λ is varied, determining the effects of nonzero axial magnetization.

B. Theory of superfluidity with axial magnetization

The superfluid properties of the spin-1 Bose gas may be evaluated by considering the system response to the combined global phase twist and z-spin rotation

$$\Psi \to e^{i\kappa_n\hat{\mathbf{n}}\cdot\mathbf{r}}e^{if_z\kappa_s\hat{\mathbf{n}}\cdot\mathbf{r}}\Psi. \tag{3}$$

Here $\hat{\mathbf{n}}$ is a unit vector defining the twist direction. This transformation modifies the kinetic energy of the gas while leaving the remaining energy terms unchanged. The transformation (3) acting on an equilibrium gas transforms the free energy to

$$F = F_0 + \int d\mathbf{r}\left(\rho_{nn}\frac{\hbar^2\kappa_n^2}{2M} + \rho_{ss}\frac{\hbar^2\kappa_s^2}{2M} + \rho_{ns}\frac{\hbar^2\kappa_n\kappa_s}{M}\right), \tag{4}$$

with F_0 the free energy prior to the transformation. In a system of dimensions $L \times L$ one has

$$\rho_{ij} \equiv \frac{M}{\hbar^2L^2}\frac{\partial^2F}{\partial\kappa_i\partial\kappa_j}\bigg|_{\kappa_i=\kappa_j=0}, \quad i,j \in \{n,s\}. \tag{5}$$

The coefficients ρ_{nn} and ρ_{ss} define the mass and spin superfluid densities, respectively.

The coefficient $\rho_{ns} = \rho_{sn}$ arises from interdependence of mass and spin currents in the presence of nonzero axial magnetization $\langle F_z\rangle$. To elucidate this, we write the free energy (4) as a function of the superfluid velocities $\mathbf{v}_i(\mathbf{r}) = (\hbar\kappa_i/M)\hat{\mathbf{n}}$. Taking functional derivatives of the free energy with respect to these velocities, one obtains the equilibrium superfluid currents as [47]

$$\langle\mathbf{j}_n\rangle = \frac{\delta F}{\delta\mathbf{v}_n} = \rho_{nn}\mathbf{v}_n + \rho_{ns}\mathbf{v}_s, \quad \langle\mathbf{j}_s\rangle = \frac{\delta F}{\delta\mathbf{v}_s} = \rho_{ss}\mathbf{v}_s + \rho_{ns}\mathbf{v}_n. \tag{6}$$

Motivated by Eq. (6) we interpret ρ_{ns} as the portion of mass (spin) superfluid density that simultaneously contributes to spin (mass) superflow. Note $F - F_0 \geqslant 0$ irrespective of κ_n and κ_s; hence $\rho_{ns} \leqslant \sqrt{\rho_{nn}\rho_{ss}}$. The coupling arises due to the interdependence of the two symmetry transformations, whereby spin rotations affect mass current and global phase rotations affect spin current. A quantity analogous to ρ_{ns} arises in two-component superfluids, where it is termed the superfluid drag; this describes entrainment between the two components due to current-current coupling, known as the Andreev-Bashkin effect [39]. Note ρ_{ns} is distinct from the effect termed "spin

drag" in Ref. [29], which describes the tendency for component currents to entrain due to the spin exchange energy.

The total instantaneous mass and spin currents in the spinor system are, respectively [48],

$$\mathbf{J}_n = \frac{\hbar}{M}\mathrm{Im}(\Psi^\dagger \nabla \Psi), \quad \mathbf{J}_s = \frac{\hbar}{M}\mathrm{Im}(\Psi^\dagger f_z \nabla \Psi). \tag{7}$$

At zero temperature the total and superfluid currents are identical. Applying the transformation (3) to the spatially uniform ground state and evaluating Eq. (7) we identify

$$\begin{aligned} \rho_{nn} &= n, \\ \rho_{ss} &= |\psi_1|^2 + |\psi_{-1}|^2 \quad \text{(zero temperature)}, \\ \rho_{ns} &= F_z. \end{aligned} \tag{8}$$

At zero temperature, the superfluid densities ρ_{nn} and ρ_{ns} are distinct in the broken-axis symmetric phase $\lambda < q$, but become equal in the easy-axis phase $\lambda \geqslant q$, where $|\psi_0|^2 = |\psi_{-1}|^2 = 0$ and $F_z = n$.

C. Model and simulation details

We consider a 2D spin-1 Bose gas confined to a box of dimensions $L \times L$, coupled to a grand-canonical reservoir with chemical potential μ, magnetic potential λ, and temperature T. For a given quantity $\mathcal{O}$ equilibrium expectation values are given by

$$\langle \mathcal{O} \rangle = \frac{1}{Z}\int D\Psi\, \mathcal{O}[\Psi] e^{-(E[\Psi]-\mu N[\Psi]-\lambda M_z[\Psi])/k_B T}, \tag{9}$$

where $Z = \int D\Psi\, \exp[-(E - \mu N - \lambda M_z)/k_B T]$ is the system partition function. In practice, we evaluate Eq. (9) from stationary solutions of the stochastic spin-1 Gross-Pitaevskii equation, which sample the grand-canonical ensemble [36] (also see Refs. [49,50]). This equation is [33–37]

$$i\hbar\, d\Psi = (1 - i\gamma)[\mathcal{L}\{\Psi\} - (\mu + \lambda f_z)\Psi]dt + i\hbar\, dW. \tag{10}$$

The nonlinear operator

$$\mathcal{L}\{\Psi\} = \left(-\frac{\hbar^2\nabla^2}{2M} + q f_z + g_n n + g_s \sum_\nu F_\nu f_\nu\right)\Psi \tag{11}$$

describes time evolution due to kinetic energy, quadratic Zeeman shift, density-dependent interactions, and spin-dependent interactions ($\nu \in \{x, y, z\}$). The dimensionless parameter γ describes the coupling strength between Ψ and the grand canonical reservoir; stationary solutions are independent of γ. The components of $dW = [dw_1, dw_0, dw_{-1}]^T$ are circularly symmetric Gaussian-distributed complex noise with correlations $\langle dw_m^*(\mathbf{r}) dw_{m'}(\mathbf{r}')\rangle = (2\gamma k_B T/\hbar)\tilde{\delta}(\mathbf{r}, \mathbf{r}')\delta_{m,m'}dt$, where $\tilde{\delta}$ is a delta function in the space of macroscopically occupied modes [36].

We perform simulations with periodic boundary conditions. We expand the field Ψ in a plane-wave basis, with the constituent modes determined by our $\mathcal{N} \times \mathcal{N}$ point numerical grid. At large momenta interactions are unimportant, so that a mode of wave number k will have occupation $N_k \approx 2Mk_BT/\hbar^2k^2$. Motivated by this we set $\Delta x = L/\mathcal{N} = \lambda_{\mathrm{th}}$ with $\lambda_{\mathrm{th}} = \sqrt{2\pi\hbar^2/Mk_BT}$ the thermal de Broglie wavelength. This ensures occupation of at least order unity for all modes after adjusting for our use of a square grid [51]. We take μ as an energy scale with associated length $x_\mu = \hbar/\sqrt{M\mu}$ and compute dependence of equilibrium properties on the scaled temperature $\mathcal{T} = Mg_nk_BT/\hbar^2\mu$ and magnetic potential λ/μ. The scaled temperature $\mathcal{T}$ captures the dependence of thermodynamic properties on both temperature and chemical potential [52,53]. Hereon, the remaining parameters are fixed as $Mg_n/\hbar^2 = 0.15$, $g_s = -0.1g_n$, $q = 0.1\mu$, and $\gamma = 0.1$, unless otherwise stated.

We obtain stationary solutions of Eq. (10) by evolving an initial state $\Psi = 0$ for time $t \sim 10^5\hbar/\mu$, observing saturation of the zero momentum mode population to verify equilibration is reached. Following this, we obtain $\mathcal{N}_s \sim 5 \times 10^4$ samples Ψ_i at intervals of $10\hbar/\mu$ and compute thermal expectation values via

$$\langle \mathcal{O} \rangle \approx \frac{1}{\mathcal{N}_s}\sum_{i=1}^{\mathcal{N}_s} \mathcal{O}[\Psi_i]. \tag{12}$$

Validity of this stochastic Gross-Pitaevskii model requires that all modes within Ψ have occupation of at least order unity and that Ψ contains all interacting modes (those with wave number $|\mathbf{k}| \leqslant x_\mu^{-1}$). These requirements may be simultaneously satisfied only if $k_BT \geqslant \mu$. For this reason we restrict our computations to temperatures $\mathcal{T} \geqslant 0.05$. We note this condition on T is equivalently stated as $\lambda_{\mathrm{th}} \lesssim x_\mu$; as we take $\Delta x = \lambda_{\mathrm{th}}$, this ensures resolution of the length scale x_μ.

III. NUMERICAL RESULTS

A. Superfluid phases in the presence of axial magnetization

We first explore the change in superfluid properties of the system as the scaled temperature $\mathcal{T}$ and magnetic potential λ are varied. Recent works [28,29] focusing on the unmagnetized case, $\lambda = 0$, found that this system exhibits two distinct BKT transitions as it is cooled. It first transitions at temperature $\mathcal{T}_n$ to a phase exhibiting only mass superfluidity, before transitioning again at a lower temperature $\mathcal{T}_s$ to a phase where both spin and mass superfluidity coexist. The difference between $\mathcal{T}_n$ and $\mathcal{T}_s$ was found to relate to the energy difference between mass and spin vortices, with $\mathcal{T}_s$ approaching $\mathcal{T}_n$ for small q/μ and approaching zero for $q \to q_0$ [29].

The superfluid densities ρ_{nn}, ρ_{ss}, and ρ_{ns}, defined in Eq. (5), can be extracted from equilibrium current-current correlations (see the Appendix for details). The dependence of these superfluid densities on both $\mathcal{T}$ and λ is shown in Figs. 2(a)–2(c). We observe three distinct superfluid phases. At low magnetization, the system behaves similarly to the $\lambda = 0$ case: there is first a transition to a mass superfluid ($\rho_{nn} > 0$) at critical temperature $\mathcal{T}_n$ [panel (a)], followed by a second transition at a lower critical temperature $\mathcal{T}_s$, where spin superfluidity ($\rho_{ss} > 0$) also emerges [panel (b)]. As λ is increased, the coupling ρ_{ns} between the two superfluids grows [panel (c)]. The spin superfluid density ρ_{ss} also grows with λ until it coincides with ρ_{nn} for $\lambda > \lambda_c(\mathcal{T})$, defining a third superfluid region. Here $\lambda_c(\mathcal{T})$ is the curve demarcating $\rho_{nn} > \rho_{ss}$ [$\lambda < \lambda_c(\mathcal{T})$] from $\rho_{nn} = \rho_{ss}$ [$\lambda \geqslant \lambda_c(\mathcal{T})$]. This crossover generalizes the zero-temperature transition from the broken axisymmetry to the easy-axis phase. We therefore denote the region where

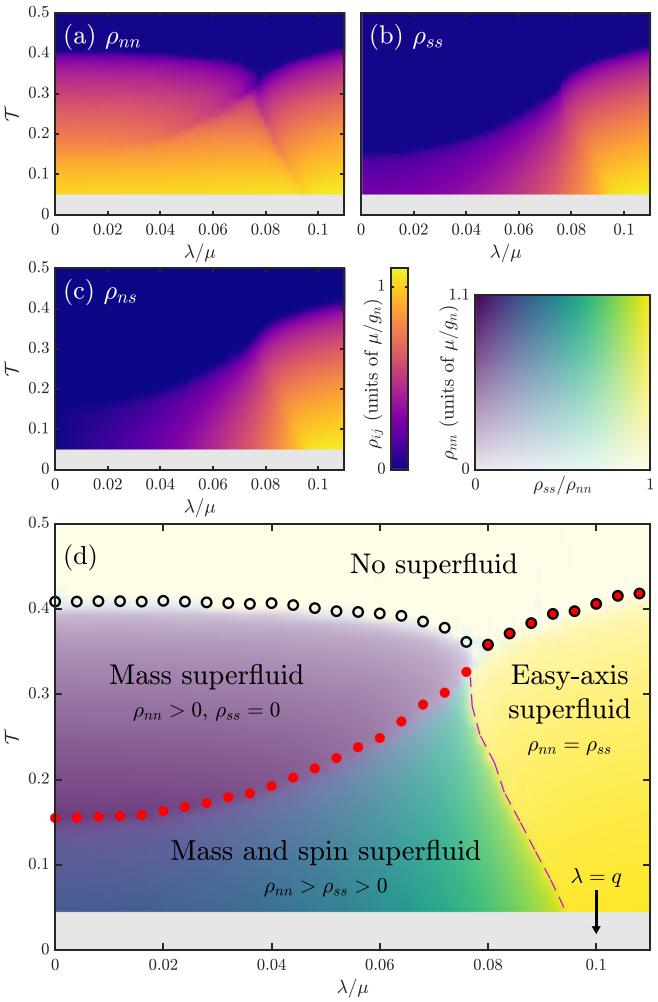

FIG. 2. Superfluid densities (a) ρ_{nn}, (b) ρ_{ss}, and (c) ρ_{ns} for varying temperature $\mathcal{T}$ and magnetic potential λ. (d) We identify three superfluid phases: first, a mass superfluid phase, with $\rho_{nn} > 0$ and $\rho_{ss} = 0$. Second, a mass and spin superfluid phase, with $\rho_{nn} > \rho_{ss} > 0$. Third, an easy-axis superfluid phase, with $\rho_{nn} = \rho_{ss} = \rho_{ns}$. Black and red circles denote approximate mass and spin superfluid transition temperatures, respectively, identified via the conditions ρ_{nn}, $\rho_{ss} > 0.05\mu/g_n$. Purple dashed line denotes the curve $\lambda_c(\mathcal{T})$, identified via the condition $\rho_{nn} - \rho_{ss} < 0.05\mu/g_n$. All results are computed with $\mathcal{N} = 256$.

$\rho_{nn} = \rho_{ss}$ an "easy-axis superfluid." The superfluid phase diagram is summarized in Fig. 2(d).

The zero temperature value of λ_c corresponds to the transition from the broken axisymmetry to the easy-axis ground state [32], i.e., $\lambda_c(0) = q$; see Fig. 2(d). At finite temperature, we find that $\lambda_c(\mathcal{T}) < \lambda_c(0)$ and the gas has only partial axial magnetization. In particular, at $\mathcal{T} = \mathcal{T}_n$ we find λ_c is determined by the condition that the component densities $n_1 = \langle|\psi_1|^2\rangle$ and $n_0 = \langle|\psi_0|^2\rangle$ are equal. In Fig. 3(a) we plot the difference $n_1 - n_0$; the intersection of the curve $n_1 = n_0$ (blue dotted line) with $\mathcal{T}_n$ (black circles) occurs at $\lambda \approx \lambda_c(\mathcal{T}_n)$. Approximating n_0 and n_1 by their broken-axisymmetric ground-state values gives an accurate analytic estimate for $\lambda_c(\mathcal{T}_n)$ [54]; see Fig. 3. We have performed additional calculations of the phase diagram for $(g_s/g_n, q/\mu) = (-0.1, 0.01)$ and $(g_s/g_n, q/\mu) = (-0.5, 0.5)$. In both cases results are qualitatively similar to Fig. 2, with $\lambda_c(\mathcal{T}_n)$ in agreement with the analytic estimate; see Figs. 3(b) and 3(c).

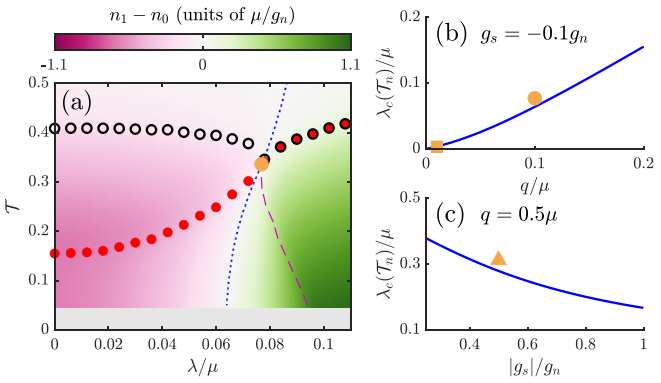

FIG. 3. Role of component densities in determining $\lambda_c(\mathcal{T}_n)$. (a) Density difference $n_1 - n_0$. Black and red circles and purple dashed line are as in Fig. 2(d). The mass and spin superfluid transitions coincide at $\lambda = \lambda_c(\mathcal{T}_n)$ (orange circle). Dotted blue line is the curve $n_1 = n_0$, which coincides with $\lambda_c(\mathcal{T}_n)$ at $\mathcal{T} = \mathcal{T}_n$. (b) Dependence of $\lambda_c(\mathcal{T}_n)$ on quadratic Zeeman energy for $g_s = -0.1g_n$. (c) Dependence of $\lambda_c(\mathcal{T}_n)$ on $|g_s|$ with $q = 0.5\mu$. In (b) and (c) blue lines are analytic estimates obtained from setting $n_1 = n_0$ in the ground state, while orange markers are numerical results with $(g_s/g_n, q/\mu) = (-0.1, 0.1)$ (circle), $(-0.1, 0.01)$ (square), and $(-0.5, 0.5)$ (triangle). All results are computed with $\mathcal{N} = 256$.

B. Phase coherence and correlations

Superfluidity in two dimensions is associated with algebraic decay of correlations, signifying quasi-long-range order. In a spinor system, such order may be present in component ψ_m and spin $\mathbf{F}_\perp = (F_x, F_y)$ correlations

$$G_m(\mathbf{r}) = \langle\psi_m^*(\mathbf{r})\psi_m(\mathbf{0})\rangle, \quad G_\perp(\mathbf{r}) = \langle\mathbf{F}_\perp(\mathbf{r})\cdot\mathbf{F}_\perp(\mathbf{0})\rangle. \quad (13)$$

At low temperature the behavior of these correlations is dominated by long-wavelength gapless modes [11]. This system exhibits two such modes, corresponding to the two symmetries in Eq. (3) [55,56]. Excitations of these modes are described via the energy functional

$$E = \frac{\hbar^2}{2M}\int d\mathbf{r}(\rho_{nn}|\nabla\theta|^2 + \rho_{ss}|\nabla\alpha|^2 + 2\rho_{ns}\nabla\theta\cdot\nabla\alpha), \quad (14)$$

where $\theta(\mathbf{r})$ and $\alpha(\mathbf{r})$ are the spatially varying global phase and transverse spin angle, respectively. The effect of these excitations on the large $|\mathbf{r}|$ behavior of the correlations (13) can be evaluated analytically from Eq. (9) using standard techniques [57,58]. Within the mass and spin superfluid phase the result is

$$G_\nu(\mathbf{r}) \propto |\mathbf{r}|^{-\eta_\nu}, \quad \nu \in \{1, 0, -1, \perp\}, \quad (15)$$

with

$$\eta_0 = \frac{Mk_BT}{2\pi\hbar^2\rho_{nn}}\frac{1}{1-\mathcal{R}^2}, \quad \eta_\perp = \frac{Mk_BT}{2\pi\hbar^2\rho_{ss}}\frac{1}{1-\mathcal{R}^2},$$
$$\eta_{\pm1} = \eta_0 + \eta_\perp \mp \frac{Mk_BT}{\pi\hbar^2\sqrt{\rho_{nn}\rho_{ss}}}\frac{\mathcal{R}}{1-\mathcal{R}^2}, \quad (16)$$

with $\mathcal{R} = \rho_{ns}/\sqrt{\rho_{nn}\rho_{ss}}$. Note that $\eta_1 + \eta_{-1} = 2\eta_\perp + 2\eta_0$ and hence only three of the four exponents in Eq. (16) are independent. Equation (16) can be written concisely as

$$\eta = \frac{Mk_BT}{2\pi\hbar^2}\rho^{-1}, \tag{17}$$

where we have defined

$$\eta = \begin{bmatrix} \eta_0 & -\bar{\eta} \\ -\bar{\eta} & \eta_\perp \end{bmatrix}, \quad \rho = \begin{bmatrix} \rho_{nn} & \rho_{ns} \\ \rho_{ns} & \rho_{ss} \end{bmatrix}, \tag{18}$$

with $\bar{\eta} = (\eta_{-1} - \eta_1)/4$.

In the easy-axis superfluid phase $\mathcal{R} = 1$ and the expressions (16) are invalid. Rather, we note that with $\rho_{nn} = \rho_{ss} = \rho_{ns}$ Eq. (14) reduces to $E = (\hbar^2/2M)\int d\mathbf{r}\rho_{ns}|\nabla(\theta+\alpha)|^2$, i.e., the energy reduces to that of a single-component field with fluctuations in the phase $\theta + \alpha$. Correspondingly, the only relevant correlation function is $G_1(\mathbf{r}) \propto |\mathbf{r}|^{-\eta_1}$ with decay exponent satisfying

$$\eta_1 = \frac{Mk_BT}{2\pi\hbar^2\rho_{ns}} \quad \text{(easy-axis superfluid)}. \tag{19}$$

Similarly, in the mass superfluid phase $\rho_{ss} = \rho_{ns} = 0$ and Eq. (14) reduces to $E = (\hbar^2/2M)\int d\mathbf{r}\,\rho_{nn}|\nabla\theta|^2$. The relevant correlation function is then $G_0(\mathbf{r}) \propto |\mathbf{r}|^{-\eta_0}$ with decay exponent

$$\eta_0 = \frac{Mk_BT}{2\pi\hbar^2\rho_{nn}} \quad \text{(mass superfluid)}. \tag{20}$$

These results connect quasi-long-range order with superfluidity.

We have numerically determined the correlation functions (13) using Eq. (12). In the distinct mass and spin superfluid phase all G_ν exhibit algebraic decay. In the easy-axis superfluid phase only G_1 exhibits algebraic decay. In the mass superfluid phase only G_0 exhibits algebraic decay. Example correlations are shown in Figs. 4(a) and 4(b). We have also computed the long-range behavior of G_ν from the superfluid densities using Eq. (15) with decay exponents as in Eqs. (16), (19), and (20). This agrees with the correlations determined directly within the long-wavelength region $10\lambda_{\text{th}} < |\mathbf{r}| < 0.2L$. The upper bound of $0.2L$ is imposed as finite-size effects become significant for $|\mathbf{r}| > 0.2L$.

Similarly, we have extracted the decay exponents η_ν from correlations computed via Eq. (12) [59] and compared these with the predictions (16), (19), and (20); see Figs. 4(c) and 4(d). We find agreement for all applicable temperatures. Interestingly, in the distinct mass and spin superfluid phase, where all G_ν exhibit algebraic decay, we find the decay exponents η_ν may exceed $1/4$. This is in contrast to the maximal decay exponent of a single-component 2D superfluid [60].

Conversely, we may express the superfluid densities in terms of the decay exponents. In the easy-axis and mass superfluid phases this is achieved directly via Eqs. (19) and (20). In the mass and spin superfluid phase, inverting Eq. (17) gives

$$\rho_{nn} = \frac{Mk_BT}{2\pi\hbar^2\eta_0}\frac{1}{1-\mathcal{E}^2}, \quad \rho_{ss} = \frac{Mk_BT}{2\pi\hbar^2\eta_\perp}\frac{1}{1-\mathcal{E}^2},$$
$$\rho_{ns} = \frac{Mk_BT}{2\pi\hbar^2\sqrt{\eta_\perp\eta_0}}\frac{\mathcal{E}}{1-\mathcal{E}^2}, \tag{21}$$

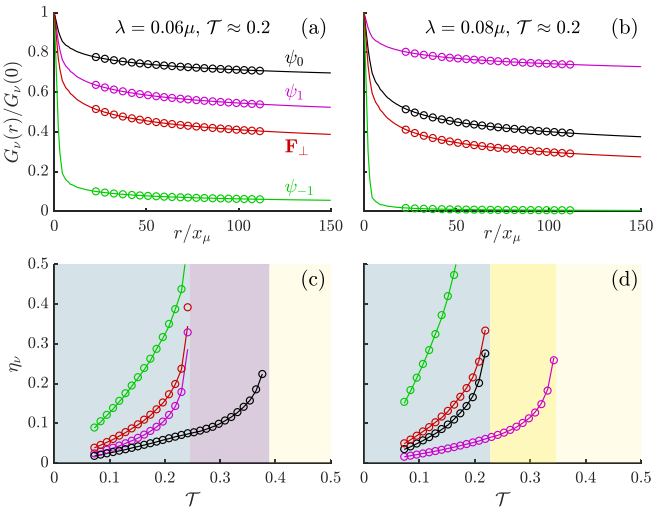

FIG. 4. Top row: algebraically decaying correlations G_1 (purple), G_0 (black), G_{-1} (green), and $G_\perp$ (red), at $\mathcal{T} \approx 0.2$ with (a) $\lambda = 0.06\mu$ and (b) $\lambda = 0.08\mu$. Lines are obtained from evaluation of Eq. (13). Circles are obtained from Eq. (15) with decay exponents as in Eqs. (16), (19), and (20) and superfluid densities computed numerically from equilibrium current-current correlations. Bottom row: comparison of decay exponents η_ν extracted from fitting to correlations (13) (lines) and decay exponents computed from superfluid densities (16), (19), and (20) (circles), with (c) $\lambda = 0.06\mu$ and (d) $\lambda = 0.08\mu$. Colors are as in (a) and (b). Background colors indicate superfluid phases from Fig. 2(d). All results are computed with $\mathcal{N} = 512$.

with $\mathcal{E} = \bar{\eta}/\sqrt{\eta_\perp\eta_0}$. In Fig. 5 we compare superfluid densities extracted from equilibrium current-current correlations (circles) to those computed from Eqs. (19)–(21), with decay exponents extracted from fits to correlations (13) (dots). We find agreement at all temperatures for multiple values of λ. The relations (21) illustrate the effect of ρ_{ns} on the mass and spin superfluid densities. In particular, the emergence of ρ_{ns} results in a two-step transition in the mass superfluidity; see Figs. 5(b) and 5(c). These steepen with increasing system size, see Fig. 6 in the Appendix, and resemble the universal jump in superfluidity that occurs in single-component systems [23,60]. Future work could investigate in more detail the finite-size scaling of these to verify their behavior in the thermodynamic limit.

IV. CONCLUSION

In this paper we investigated the effect of axial magnetization on the superfluid properties of a ferromagnetic spin-1 Bose gas in two dimensions. This system supports superfluidity of both mass and spin currents, arising via respective BKT transitions. We find that the spin superfluid transition temperature increases with increasing magnetic potential, ultimately coinciding with the mass superfluid transition temperature. We thus identify three superfluid regimes: one with only mass superfluidity, one with distinct mass and spin superfluidity, and one with identical mass and spin superfluidity.

We have quantified the interdependence of mass and spin currents at nonzero magnetic potential via the introduction

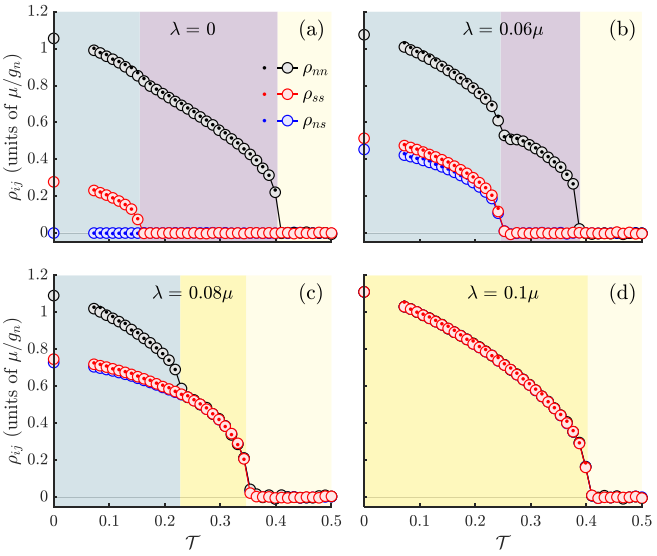

FIG. 5. Temperature dependence of superfluid densities ρ_{nn} (black), ρ_{ss} (red), and ρ_{ns} (blue) at (a) $\lambda = 0$, (b) $\lambda = 0.06\mu$, (c) $\lambda = 0.08\mu$, and (d) $\lambda = 0.1\mu$. Circles are evaluated via the procedure described in the Appendix. Dots are evaluated via decay exponents η_v extracted from fits to algebraically decaying correlations G_v (see text). Zero temperature points are computed via Eq. (8). Background colors indicate superfluid phases from Fig. 2(d). All results are computed with $\mathcal{N} = 512$.

of a third superfluid quantity, ρ_{ns}. This quantity is analogous to the superfluid drag present in binary superfluids which, as with the system considered here, exhibit a U(1) × U(1) symmetry. However, we note an important distinction: the two superflows exhibited by the binary fluid correspond directly to transport of the individual fluid components, with superfluid drag describing entrainment between them. Contrarily, the two superflows exhibited by the broken-axisymmetric spin-1 Bose gas are associated with transport of mass and axial magnetization, with ρ_{ns} quantifying the extent to which these superflows are identical; the mass and spin superfluid currents

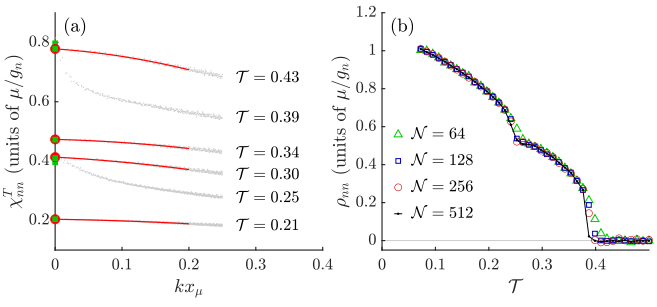

FIG. 6. Attainment of mass superfluid density at $\lambda = 0.06\mu$. (a) Wave-number dependence of transverse response function χ^T_{nn} (gray dots). Red lines are fits used to extract the $k \to 0$ limit. Green squares indicate values computed via squared momentum expectations; see text. (b) Temperature dependence of mass superfluid density obtained with system sizes $\mathcal{N} = 64$, 128, 256, and 512. Note the two-step transition in ρ_{nn}, which steepens with increasing system size.

do not correspond to flow of distinct "mass" and "spin" fluid components.

We have presented the relationship between the relevant correlations and superfluidity in the presence of axial magnetization. Recent work on spatially resolved measurement of collective spin observables and the associated correlation functions in quasi-1D spin-1 gases [16,17] should be applicable to the 2D regime considered here. Axial magnetization will affect the nature of vortices in this system [61–63]; exploring this in the context of the BKT transitions identified in this work would be an interesting area to explore.

ACKNOWLEDGMENTS

X.Y. acknowledges support from the National Natural Science Foundation of China (Grant No. 12175215), the National Key Research and Development Program of China (Grants No. 2022YFA and No. 1405300), and NSAF (Grant No. U2330401). A.P.C.U. and P.B.B. acknowledge support from the Marsden Fund of the Royal Society of New Zealand. This research was supported by the Australian Research Council Centre of Excellence for Engineered Quantum Systems (EQUS, Grant No. CE170100009) and the Australian government Department of Industry, Science, and Resources via the Australia-India Strategic Research Fund (Grant No. AIRXIV000025). This research was partially supported by the Australian Research Council Centre of Excellence in Future Low-Energy Electronics Technologies (Project No. CE170100039) and funded by the Australian Government. The authors wish to acknowledge the use of New Zealand eScience Infrastructure (NeSI) high performance computing facilities as part of this research.

APPENDIX: COMPUTING SUPERFLUID DENSITIES

To compute the definitions (5) we consider the free energy $F = -k_B T \ln Z$, where the partition function

$$Z = \int d\Psi \, \exp\left[-(E - \mu N - \lambda M_z)/k_B T\right] \tag{A1}$$

is evaluated over states Ψ satisfying periodic boundary conditions, with the effect of the phase twist (3) incorporated into the state energy via the transformation

$$E = E_0 + \sum_{i,j} \frac{\hbar^2 \kappa_i \kappa_j}{2M} N_{ij} + \hbar \int d\mathbf{r} (\kappa_n \mathbf{J}_n + \kappa_s \mathbf{J}_s) \cdot \hat{\mathbf{n}}. \tag{A2}$$

Here E_0 is the energy prior to the transformation (1), $N_{ij} = \int d\mathbf{r}\, \Psi^\dagger A_i A_j \Psi$, $A_n = \mathbb{1}$, $A_s = f_z$, and $\mathbf{J}_i$ are the total currents (7). Substituting Eq. (A2) into Eq. (A1) and computing Eq. (5) from the free energy gives

$$\rho_{ij} = n_{ij} - \frac{M}{k_B T L^2} \int d\mathbf{r} \int d\mathbf{r}' \hat{\mathbf{n}} \cdot \langle \mathbf{J}_i(\mathbf{r}) \mathbf{J}_j(\mathbf{r}') \rangle \cdot \hat{\mathbf{n}}, \tag{A3}$$

where $n_{ij} = \langle N_{ij} \rangle / L^2$ and $\mathbf{J}_i(\mathbf{r})\mathbf{J}_j(\mathbf{r}')$ denotes the outer product of $\mathbf{J}_i(\mathbf{r})$ and $\mathbf{J}_j(\mathbf{r}')$. Note that the mass and spin momenta are $P_i = M \int d\mathbf{r}\, \mathbf{J}_i \cdot \hat{\mathbf{n}}$ and hence Eq. (A3) can also be written as [64]

$$\rho_{ij} = n_{ij} - \frac{\langle P_i P_j \rangle}{M L^2 k_B T}. \tag{A4}$$

In the infinite system size limit the current-current correlation function $\langle \mathbf{J}_i(\mathbf{r})\mathbf{J}_j(\mathbf{r}') \rangle$ depends only on the separation $\mathbf{r} - \mathbf{r}'$.

With this one may express Eq. (A3) as

$$\rho_{ij} = n_{ij} - \lim_{L^2\to\infty} \int d\mathbf{k}\, \Delta(\mathbf{k})[\hat{\mathbf{n}} \cdot \chi_{ij}(\mathbf{k}) \cdot \hat{\mathbf{n}}], \tag{A5}$$

where $\Delta(\mathbf{k}) \equiv \int d\mathbf{r} \frac{1}{4\pi^2} e^{i\mathbf{k}\cdot\mathbf{r}}$ and

$$\chi_{ij}(\mathbf{k}) \equiv \frac{M}{k_B T L^2} \langle \tilde{\mathbf{J}}_i(\mathbf{k}) \tilde{\mathbf{J}}_j^*(\mathbf{k}) \rangle, \tag{A6}$$

with $\tilde{\mathbf{J}}_i(\mathbf{k}) = \int d\mathbf{r}\, e^{-i\mathbf{k}\cdot\mathbf{r}} \mathbf{J}_i(\mathbf{r})$.

The function $\Delta(\mathbf{k})$ approaches a delta function in the infinite system size limit $L^2 \to \infty$. However, the way in which this limit is taken is of critical importance. Consider the fluid to be confined within a rectangular box of dimensions $L_n \times L_m$ with walls oriented along perpendicular directions $\hat{\mathbf{n}}$ and $\hat{\mathbf{m}}$. To probe superfluidity, one must take the limit $L_n \to \infty$ first (see, for example, Ref. [65]). The function $\Delta(\mathbf{k})$ then acts to ensure the integration is performed over $\mathbf{k} \perp \hat{\mathbf{n}}$, so that $\hat{\mathbf{n}} \cdot \chi_{ij}(\mathbf{k}) \cdot \hat{\mathbf{n}} = \chi_{ij}^T(|\mathbf{k}|)$ gives the transverse response. Alternatively, taking first $L_m \to \infty$ results in integration over $\mathbf{k} \parallel \hat{\mathbf{n}}$ so that $\hat{\mathbf{n}} \cdot \chi_{ij}(\mathbf{k}) \cdot \hat{\mathbf{n}} = \chi_{ij}^L(|\mathbf{k}|)$ gives the longitudinal response, satisfying $\chi_{ij}^L(0) = n_{ij}$. With these considerations one obtains

$$\rho_{ij} = \lim_{|\mathbf{k}|\to 0} \left[\chi_{ij}^L(|\mathbf{k}|) - \chi_{ij}^T(|\mathbf{k}|)\right]. \tag{A7}$$

We compute superfluid densities via Eq. (A7). Away from transition temperatures a quadratic fit to the response functions $\chi_{ij}^L(|\mathbf{k}|)$ and $\chi_{ij}^T(|\mathbf{k}|)$ is sufficient to extract the $|\mathbf{k}| \to 0$ limit; see Fig. 6(a). However, near transition temperatures the response function $\chi_{ij}^T(|\mathbf{k}|)$ changes rapidly near $\mathbf{k} = \mathbf{0}$ and the fitting procedure becomes unreliable. We therefore compute the $|\mathbf{k}| \to 0$ limit via $\lim_{|\mathbf{k}|\to 0} \chi_{ij}^T(|\mathbf{k}|) \to \langle P_i P_j \rangle / ML^2 k_B T$; cf. Eq. (A4).

We have computed superfluid densities on $\mathcal{N} \times \mathcal{N}$ point numerical grids with $\mathcal{N} = 64$, 128, 256, and 512. Example results are shown in Fig. 6(b). System-size dependence is observed near superfluid transition temperatures.

[1] T.-L. Ho, Spinor Bose condensates in optical traps, Phys. Rev. Lett. **81**, 742 (1998).

[2] T. Ohmi and K. Machida, Bose-Einstein condensation with internal degrees of freedom in alkali atom gases, J. Phys. Soc. Jpn. **67**, 1822 (1998).

[3] J. Stenger, S. Inouye, D. M. Stamper-Kurn, H.-J. Miesner, A. P. Chikkatur, and W. Ketterle, Spin domains in ground-state Bose–Einstein condensates, Nature (London) **396**, 345 (1998).

[4] Y. Kawaguchi and M. Ueda, Spinor Bose–Einstein condensates, Phys. Rep. **520**, 253 (2012).

[5] L. E. Sadler, J. M. Higbie, S. R. Leslie, M. Vengalattore, and D. M. Stamper-Kurn, Spontaneous symmetry breaking in a quenched ferromagnetic spinor Bose–Einstein condensate, Nature (London) **443**, 312 (2006).

[6] J. Guzman, G.-B. Jo, A. N. Wenz, K. W. Murch, C. K. Thomas, and D. M. Stamper-Kurn, Long-time-scale dynamics of spin textures in a degenerate $F = 1^{87}$ Rb spinor Bose gas, Phys. Rev. A **84**, 063625 (2011).

[7] A. Lamacraft, Quantum quenches in a spinor condensate, Phys. Rev. Lett. **98**, 160404 (2007).

[8] B. Damski and W. H. Zurek, Dynamics of a quantum phase transition in a ferromagnetic Bose-Einstein condensate, Phys. Rev. Lett. **99**, 130402 (2007).

[9] H. Saito, Y. Kawaguchi, and M. Ueda, Kibble-Zurek mechanism in a quenched ferromagnetic Bose-Einstein condensate, Phys. Rev. A **76**, 043613 (2007).

[10] M. Anquez, B. A. Robbins, H. M. Bharath, M. Boguslawski, T. M. Hoang, and M. S. Chapman, Quantum Kibble-Zurek mechanism in a spin-1 Bose-Einstein condensate, Phys. Rev. Lett. **116**, 155301 (2016).

[11] R. Barnett, A. Polkovnikov, and M. Vengalattore, Prethermalization in quenched spinor condensates, Phys. Rev. A **84**, 023606 (2011).

[12] L. A. Williamson and P. B. Blakie, Universal coarsening dynamics of a quenched ferromagnetic spin-1 condensate, Phys. Rev. Lett. **116**, 025301 (2016).

[13] L. A. Williamson and P. B. Blakie, Anomalous phase ordering of a quenched ferromagnetic superfluid, SciPost Phys. **7**, 029 (2019).

[14] C.-M. Schmied, M. Prüfer, M. K. Oberthaler, and T. Gasenzer, Bidirectional universal dynamics in a spinor Bose gas close to a nonthermal fixed point, Phys. Rev. A **99**, 033611 (2019).

[15] I. Siovitz, S. Lannig, Y. Deller, H. Strobel, M. K. Oberthaler, and T. Gasenzer, Universal dynamics of rogue waves in a quenched spinor Bose condensate, Phys. Rev. Lett. **131**, 183402 (2023).

[16] M. Prüfer, P. Kunkel, H. Strobel, S. Lannig, D. Linnemann, C.-M. Schmied, J. Berges, T. Gasenzer, and M. K. Oberthaler, Observation of universal dynamics in a spinor Bose gas far from equilibrium, Nature (London) **563**, 217 (2018).

[17] M. Prüfer, D. Spitz, S. Lannig, H. Strobel, J. Berges, and M. K. Oberthaler, Condensation and thermalization of an easy-plane ferromagnet in a spinor Bose gas, Nat. Phys. **18**, 1459 (2022).

[18] S. Kang, S. W. Seo, J. H. Kim, and Y. Shin, Emergence and scaling of spin turbulence in quenched antiferromagnetic spinor Bose-Einstein condensates, Phys. Rev. A **95**, 053638 (2017).

[19] N. D. Mermin and H. Wagner, Absence of ferromagnetism or antiferromagnetism in one- or two-dimensional isotropic Heisenberg models, Phys. Rev. Lett. **17**, 1133 (1966).

[20] P. C. Hohenberg, Existence of long-range order in one and two dimensions, Phys. Rev. **158**, 383 (1967).

[21] V. L. Berezinskii, Destruction of long-range order in one-dimensional and two-dimensional systems having a continuous symmetry group I. classical systems, Sov. Phys. JETP **32**, 493 (1971).

[22] J. M. Kosterlitz and D. J. Thouless, Ordering, metastability and phase transitions in two-dimensional systems, J. Phys. C: Solid State Phys. **6**, 1181 (1973).

[23] D. J. Bishop and J. D. Reppy, Study of the superfluid transition in two-dimensional ^{4}He films, Phys. Rev. Lett. **40**, 1727 (1978).

[24] S. Mukerjee, C. Xu, and J. E. Moore, Topological defects and the superfluid transition of the $s = 1$ spinor condensate in two dimensions, Phys. Rev. Lett. **97**, 120406 (2006).

[25] D. Podolsky, S. Chandrasekharan, and A. Vishwanath, Phase transitions of $s = 1$ spinor condensates in an optical lattice, Phys. Rev. B **80**, 214513 (2009).

[26] V. Pietilä, T. P. Simula, and M. Möttönen, Finite-temperature phase transitions in quasi-two-dimensional spin-1 Bose gases, Phys. Rev. A **81**, 033616 (2010).

[27] A. J. A. James and A. Lamacraft, Phase diagram of two-dimensional polar condensates in a magnetic field, Phys. Rev. Lett. **106**, 140402 (2011).

[28] M. Kobayashi, Berezinskii–Kosterlitz–Thouless transition of spin-1 spinor Bose gases in the presence of the quadratic Zeeman effect, J. Phys. Soc. Jpn. **88**, 094001 (2019).

[29] A. P. C. Underwood, A. J. Groszek, X. Yu, P. B. Blakie, and L. A. Williamson, Berezinskii-Kosterlitz-Thouless transitions in an easy-plane ferromagnetic superfluid, Phys. Rev. Res. **5**, L012045 (2023).

[30] J. Armaitis and R. A. Duine, Superfluidity and spin superfluidity in spinor Bose gases, Phys. Rev. A **95**, 053607 (2017).

[31] E. B. Sonin, Spin and mass superfluidity in a ferromagnetic spin-1 Bose-Einstein condensate, Phys. Rev. B **97**, 224517 (2018).

[32] K. Murata, H. Saito, and M. Ueda, Broken-axisymmetry phase of a spin-1 ferromagnetic Bose-Einstein condensate, Phys. Rev. A **75**, 013607 (2007).

[33] C. W. Gardiner, J. R. Anglin, and T. I. A. Fudge, The stochastic Gross-Pitaevskii equation, J. Phys. B: At. Mol. Opt. Phys. **35**, 1555 (2002).

[34] C. W. Gardiner and M. J. Davis, The stochastic Gross–Pitaevskii equation: II, J. Phys. B: At. Mol. Opt. Phys. **36**, 4731 (2003).

[35] A. S. Bradley, C. W. Gardiner, and M. J. Davis, Bose-Einstein condensation from a rotating thermal cloud: Vortex nucleation and lattice formation, Phys. Rev. A **77**, 033616 (2008).

[36] P. B. Blakie, A. Bradley, M. Davis, R. Ballagh, and C. Gardiner, Dynamics and statistical mechanics of ultra-cold Bose gases using c-field techniques, Adv. Phys. **57**, 363 (2008).

[37] A. S. Bradley and P. B. Blakie, Stochastic projected Gross-Pitaevskii equation for spinor and multicomponent condensates, Phys. Rev. A **90**, 023631 (2014).

[38] T.-L. Ho and V. B. Shenoy, Local spin-gauge symmetry of the Bose-Einstein condensates in atomic gases, Phys. Rev. Lett. **77**, 2595 (1996).

[39] A. F. Andreev and E. P. Bashkin, Three-velocity hydrodynamics of superfluid solutions, Sov. Phys.-JETP **42**, 164 (1976).

[40] D. V. Fil and S. I. Shevchenko, Nondissipative drag of superflow in a two-component Bose gas, Phys. Rev. A **72**, 013616 (2005).

[41] J. Nespolo, G. E. Astrakharchik, and A. Recati, Andreev–Bashkin effect in superfluid cold gases mixtures, New J. Phys. **19**, 125005 (2017).

[42] D. Romito, C. Lobo, and A. Recati, Linear response study of collisionless spin drag, Phys. Rev. Res. **3**, 023196 (2021).

[43] D. M. Stamper-Kurn and M. Ueda, Spinor Bose gases: Symmetries, magnetism, and quantum dynamics, Rev. Mod. Phys. **85**, 1191 (2013).

[44] H. Schmaljohann, M. Erhard, J. Kronjäger, M. Kottke, S. van Staa, L. Cacciapuoti, J. J. Arlt, K. Bongs, and K. Sengstock, Dynamics of $F = 2$ spinor Bose–Einstein condensates, Phys. Rev. Lett. **92**, 040402 (2004).

[45] M.-S. Chang, C. D. Hamley, M. D. Barrett, J. A. Sauer, K. M. Fortier, W. Zhang, L. You, and M. S. Chapman, Observation of spinor dynamics in optically trapped ^{87}Rb Bose–Einstein condensates, Phys. Rev. Lett. **92**, 140403 (2004).

[46] S. J. Huh, K. Kim, K. Kwon, and J.-Y. Choi, Observation of a strongly ferromagnetic spinor Bose-Einstein condensate, Phys. Rev. Res. **2**, 033471 (2020).

[47] B. V. Svistunov, E. S. Babaev, and N. V. Prokof'ev, *Superfluid States of Matter* (CRC Press, Boca Raton, FL, 2015).

[48] E. Yukawa and M. Ueda, Hydrodynamic description of spin-1 Bose-Einstein condensates, Phys. Rev. A **86**, 063614 (2012).

[49] P. Comaron, F. Larcher, F. Dalfovo, and N. P. Proukakis, Quench dynamics of an ultracold two-dimensional Bose gas, Phys. Rev. A **100**, 033618 (2019).

[50] N. A. Keepfer, I.-K. Liu, F. Dalfovo, and N. P. Proukakis, Phase transition dimensionality crossover from two to three dimensions in a trapped ultracold atomic Bose gas, Phys. Rev. Res. **4**, 033130 (2022).

[51] The dimensions of the momentum-space grid are $2k_{\max} \times 2k_{\max}$, where $k_{\max} = \pi/\Delta x$. Defining an average wave-number cutoff k_c via $\pi k_c^2 = (2k_{\max})^2$, we set $\hbar^2 k_c^2/2M = k_B T$ so that $N_{k_c} \approx 1$.

[52] N. Prokof'ev, O. Ruebenacker, and B. Svistunov, Critical point of a weakly interacting two-dimensional Bose gas, Phys. Rev. Lett. **87**, 270402 (2001).

[53] N. Prokof'ev and B. Svistunov, Two-dimensional weakly interacting Bose gas in the fluctuation region, Phys. Rev. A **66**, 043608 (2002).

[54] For given g_n, g_s, μ, and q the estimate $\lambda_c(\mathcal{T}_n)$ is determined as the positive root of the third-order polynomial in λ

$$\frac{q-\lambda}{q+\lambda} = \frac{1}{2}\frac{\lambda^2 - q^2 + 2q|g_s|n(\lambda)}{\lambda^2 + q^2 + 2q|g_s|n(\lambda)}, \tag{A8}$$

where $n(\lambda) = (\mu - \frac{q}{2} + \frac{\lambda^2}{2q})/(g_n - |g_s|)$.

[55] S. Uchino, M. Kobayashi, and M. Ueda, Bogoliubov theory and Lee-Huang-Yang corrections in spin-1 and spin-2 Bose-Einstein condensates in the presence of the quadratic Zeeman effect, Phys. Rev. A **81**, 063632 (2010).

[56] L. M. Symes, D. Baillie, and P. B. Blakie, Static structure factors for a spin-1 Bose-Einstein condensate, Phys. Rev. A **89**, 053628 (2014).

[57] P. M. Chaikin and T. C. Lubensky, *Principles of Condensed Matter Physics* (Cambridge University Press, New York, 1995), Vol. 10.

[58] F. Wegner, Spin-ordering in a planar classical Heisenberg model, Z. Phys. **206**, 465 (1967).

[59] We determine the presence of algebraic decay in each of the correlation functions (13) by computing a quadratic fit $\ln[G_v^{\rm fit}(r)] = a_v \ln^2(r) + b_v \ln(r) + c_v$ over the range $10\Delta x < r < 0.2L$ at each temperature. If at some point $|a_v| < 0.05$, we consider the correlations to exhibit algebraic decay. To extract the associated decay exponent η_v, we compute a linear fit $\ln[G_v^{\rm fit}(r)] = -\eta_v \ln(r) + c_v$ over the same range.

[60] D. R. Nelson and J. M. Kosterlitz, Universal jump in the superfluid density of two-dimensional superfluids, Phys. Rev. Lett. **39**, 1201 (1977).

[61] J. Lovegrove, M. O. Borgh, and J. Ruostekoski, Energetically stable singular vortex cores in an atomic spin-1 Bose-Einstein condensate, Phys. Rev. A **86**, 013613 (2012).

[62] J. Lovegrove, M. O. Borgh, and J. Ruostekoski, Stability and internal structure of vortices in spin-1 Bose-Einstein condensates with conserved magnetization, Phys. Rev. A **93**, 033633 (2016).

[63] L. A. Williamson and P. B. Blakie, Damped point-vortex model for polar-core spin vortices in a ferromagnetic spin-1 Bose-Einstein condensate, Phys. Rev. Res. **3**, 013154 (2021).

[64] E. L. Pollock and D. M. Ceperley, Path-integral computation of superfluid densities, Phys. Rev. B **36**, 8343 (1987).

[65] C. J. Foster, P. B. Blakie, and M. J. Davis, Vortex pairing in two-dimensional Bose gases, Phys. Rev. A **81**, 023623 (2010).